



Microstructure and tensile strength of aluminum/stainless steel joint welded by inertia friction and continuous drive friction

Yong Liu^{1,2} · Haiyan Zhao¹ · Yun Peng² · Xiaofei Ma³

Received: 11 February 2020 / Accepted: 13 July 2020 / Published online: 9 August 2020
© International Institute of Welding 2020

Abstract

Microstructure and mechanical properties of 6061-T6 aluminum alloy/304 stainless steel (Al/steel) joints welded by inertia friction (IFW) and continuous drive friction (CDFW) were studied comparatively. Morphology, microstructure, interfacial composition, and mechanical properties of Al/steel joints were investigated. Results showed that an intermetallic compound (IMC) reaction layer was formed at the welding interface in the CDFWed joint, and wider and clearer than that of the IFWed joint. The high concentration Si was observed at the welding interface. The grain of fully dynamic recrystallized zone (FDRZ) was below 0.1 μm in both joints, and the average width of FDRZ in the IFWed joint and CDFWed joint was about 5 μm and 2 μm , respectively. FDRZ had the high hardness, and the hardness value of IFWed joint was higher than that of CDFWed joint. The maximum tensile strength of IFWed joint was higher than that of CDFWed joint, and the reason should be related to the thickness of IMC at the welding interface.

Keywords Inertia friction welding · Continuous drive friction welding · Dissimilar joint · Microstructure · Tensile strength

1 Introduction

Aluminum alloy/stainless steel dissimilar joints can combine the advantage of both materials, and have been attracted by many industries. However, the welding of aluminum and steel is difficult due to the differences in chemical, mechanical, and thermal properties of base metals [1–3]. Many welding methods are applied, but still subject to some restrictions:

the formation of thick and brittle intermetallic causes the degradation of mechanical properties.

Friction welding is a kind of solid-state welding method with low heat input [4, 5]. Oxide films can be eliminated by the rubbing effect, and aluminum alloy will be welded with steel by the frictional heat to obtain good contact [6–8]. Heat generation in friction welding mainly depends on rotational speed and time. According to the energy supply, there are two methods: continuous drive friction welding (CDFW) and inertia friction welding (IFW) [9]. In CDFW, one part is attached to a rotating spindle and reaches to a constant rotation speed. In IFW, the rotating part is connected to a flywheel, and the rotating flywheel supplies the welding energy [10]. Previous studies have achieved joining between various metals, such as superalloy [11–13], titanium alloy [14], Al-Mg [15], Cu-Steel [16], and Al-steel [17]. The intermetallic compound (IMC) layer is controlled as thin as possible by process parameters, and its critical thickness is 1–2 μm for strong bond strength [18].

During Al and steel friction welding, Al experiences the large deformation and forms the softened region in the HAZ, and occurs the large microstructural evaluation [19, 20]. There are four microstructural change zones at the Al side: base metal, heat- and deformation-affected zone, interfacial zone, solid solution zone [21]. The friction interface sequentially

Recommended for publication by Commission III - Resistance Welding, Solid State Welding, and Allied Joining Process

- ✉ Yong Liu
liuyong1350130711@126.com
- ✉ Haiyan Zhao
hyzhao@tsinghua.edu.cn
- ✉ Yun Peng
pengyun@cisri.com.cn

¹ School of Materials Science and Engineering, Tsinghua University, Beijing 100084, China
² China Iron & Steel Research Institute Group, Beijing 100081, China
³ School of Materials Science and Engineering, Shandong University, Jinan 250061, China

experienced three friction behaviors before the initial peak torque: abrasion, slide, and stick [22].

Mechanical properties of dissimilar Al-steel friction joints are influenced by process parameters and working conditions [18]. Acceptable tensile strength and ductility could obtain through optimum process parameters [23–25]. Sebastian et al. [26] found that the bond strength showed a linear decrease with increasing the IMC thickness, but the variation in bond strength did not display a clear correlation. Dong et al. [27] found that the IMC layer of rotary friction welded 5052 aluminum alloy/304 stainless steel dissimilar joints consisted of Fe_2Al_5 and $\text{Fe}_4\text{Al}_{13}$, and cracks mainly propagated along the IMCs/5052 interface.

CDFW and IFW have the potential to weld the dissimilar materials of Al and steel. Microstructural evaluation and the control of IMC are key issues for industrial application. The aim of this study is to develop a better understanding of the characteristics of Al/steel joints welded by both methods. This research will help make a better choice to weld the dissimilar materials. The morphology, interface composition, microstructure, and hardness distribution of Al/steel joints welded by both methods were investigated.

2 Experimental procedure

2.1 Materials

Base metals were 6061-T6 aluminum alloy (Al 6061) and 304 stainless steel (SS 304) in 15-mm diameter rods. Chemical compositions of aluminum alloy and stainless steel are listed in Tables 1 and 2.

2.2 Welding process

2.2.1 Inertia friction welding (IFW)

A modified HSMZ-4 inertia friction welding was used to join aluminum alloy and stainless steel. Before welding, rod surfaces were polished by SiC papers with 800 and 1500 grit and then cleaned by acetone. Stainless steel rod was fixed in a collet which was rotating at a given angular velocity; its length was 60 mm, and the fixed length was 30 mm. Aluminum alloy rod was made immobile in a stationary jaw; its length was 75 mm, and the fixed length was 40 mm. After the spindle being accelerated to a predetermined rotational speed, the

Table 1 Chemical compositions of aluminum alloy (wt.%)

Metals	Fe	Mg	Si	Mn	Cu	Cr	Zn	Ni	Al
6061-T6	0.73	1.02	0.69	0.13	0.20	0.10	0.28	0.05	Bal.

Table 2 Chemical compositions of stainless steel (wt.%)

Metals	Fe	Mn	Si	Ni	Cr	C	S	P
SS 304	Bal.	1.51	0.44	8.21	18.14	0.05	0.02	0.03

motor cut off automatically. Then stainless steel rod rotated at high revolutions with the spindle and aluminum alloy rod moved axially under the constant axial pressure. The rotational speed of the component with spindle slowed down gradually until the welding procedure was finished. Moment of inertia was 0.16 kg m^2 . The welding process parameters were optimized as follows: the axial friction pressure (P_f) was 180 MPa, and the rotational speed (n) was 1100 rpm.

2.2.2 Continuous drive friction welding (CDFW)

The welding process includes four stages: initial friction, stable friction, parking, and forging. During the welding process, the main motor kept Al 6061 rods to maintain a constant rotation speed, and SS 304 rods moved slowly and was close to the rotating Al rod under the friction pressure. The friction heat was generated when two rods connected, and then reached the initial and stable friction stages. After the friction, the forging pressure was applied to stop the rotation, and base metals achieved welding. The welding process parameters were optimized as follows: the spindle speed was 2200 rpm, and friction pressure was 40 MPa, and friction and upset time was 12 s. The adjustable process parameter was forge pressure. The Al 6061 was the rotating axis side, and the SS 304 was the fixing axis side.

2.3 Characterization

The microstructural observation of specimen was cut perpendicular to the welding interface by the electrical discharge machine. SS 304 side was etched by a solution (2.5 mL HNO_3 and 97.5 mL ethanol), and Al 6061 side was etched by Keller's reagent (1.0 mL HF, 1.5 mL HCl, 2.5 mL HNO_3 and 95 mL H_2O). Microstructural characterization was carried out by optical microscopy (OM), scanning electron microscopy (SEM), and electron backscattered diffraction (EBSD). Micro Vickers hardness test was carried out, and the hardness measurement was done in accordance with ASTM E384-01. The indentation load was 200 g and dwell time was 10 s.

3 Results and discussion

3.1 Morphology and interface of the welded joint

Figure 1 shows the morphology of joint welded by both methods. After welding, the Al metal was extruded and

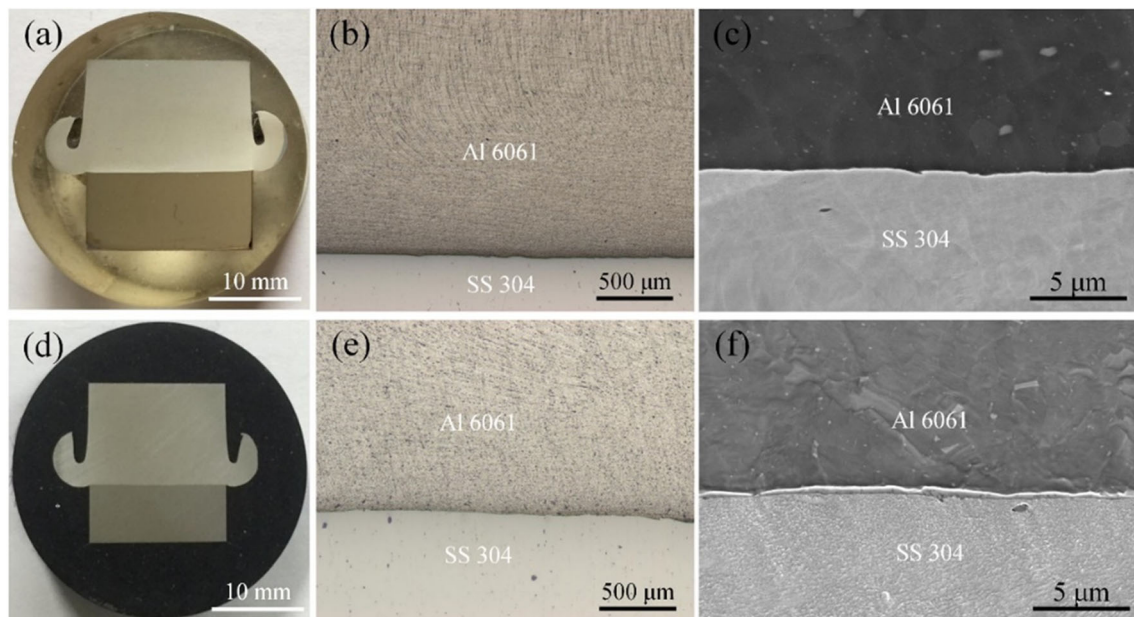


Fig. 1 Morphology and microstructure of the Al/steel joint: **a** the IFWed joint, **b** OM, and **c** SEM images of the IFWed joint, **d** the CDFWed joint, **e** OM and **f** SEM images of the CDFWed joint

caused asymmetrical deformation (Fig. 1a, d). The weld flash was formed only at the Al side. The reason should be the decrease of the tensile yield of Al 6061 with temperature during welding, and the shape of flash depended on friction welding parameters.

Al and Fe are having nearly zero mutual solubility that subsequently leads to form IMC of Fe_xAl_y . The heat distribution was non-uniform in all the directions of the interface that in turn formed a non-uniform layer of IMC. For the CDFWed joint, IMC thickness was $0.07 \mu\text{m}$ in the center of the interface; the thickness was $0.65 \mu\text{m}$ in the $1/2R$ area from the center of the interface; the thickness was $0.3 \mu\text{m}$ in the outside of the interface, as shown in Fig. 2. The reason should be that the temperature field of weld interface was not evenly distributed during welding. Compared with IFWed joint, the CDFWed joint had wider and clearer IMC layer (Fig. 1c, f). The thickness of the IMC layer of Al/steel joints was majorly depended on rotational speed and friction time [28]. This IMC layer was required as thin as possible [26, 29].

Metallurgical bonds were formed as a result of the atomic diffusion across the joint interface. The IMC layer of Al/steel joint would be formed if enough energy was provided at the weld interface. Figures 3 and 4 show elemental mapping of the Al/steel joint. It could be seen that Al, Fe, and Si elements occurred the diffusion at the weld interface and formed the IMC layer. Microstructural and elemental analysis of the joint interface showed the formation of a relatively continuous IMC layer in the CDFW joint. For the IFW joint, IMC was formed as a non-continuous morphology at the joint interface.

Nucleation and growth of IMCs were both affected by the temperature and plastic deformation at the interface. In the

both methods, variation of the rotation speeds influenced the plastic deformation and consequently the nucleation, which caused the different thickness of IMC layer.

Figures 5 and 6 are the EDS line scanning of the weld interface. The red and blue curves show the distribution of Al and Fe, respectively. The purple curve shows the distribution of Si at the interface. The high concentration level of Si was observed at the interface in both joints. The interfacial structure consisted of an IMC with Si enrichment (Figs. 5c and 6c). The local Si enrichment layer formed along the

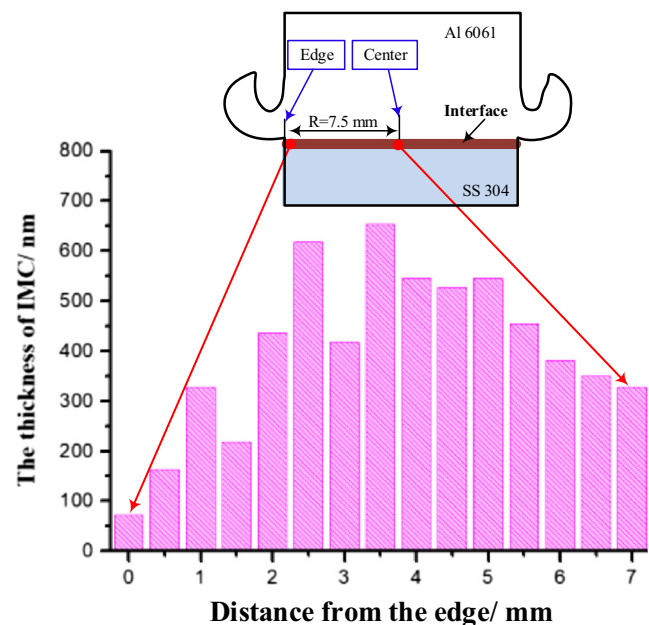


Fig. 2 The thickness of IMC in the CDFWed joint

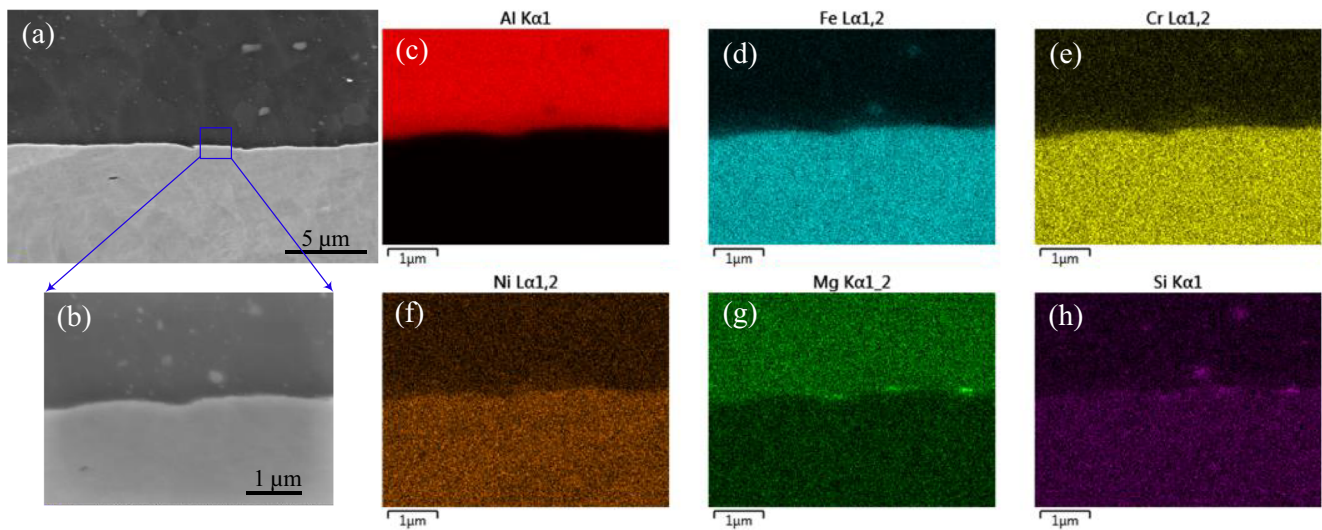


Fig. 3 a, b SEM image of the welding interface and c–h elemental mapping of Al/steel joint welded by IFW

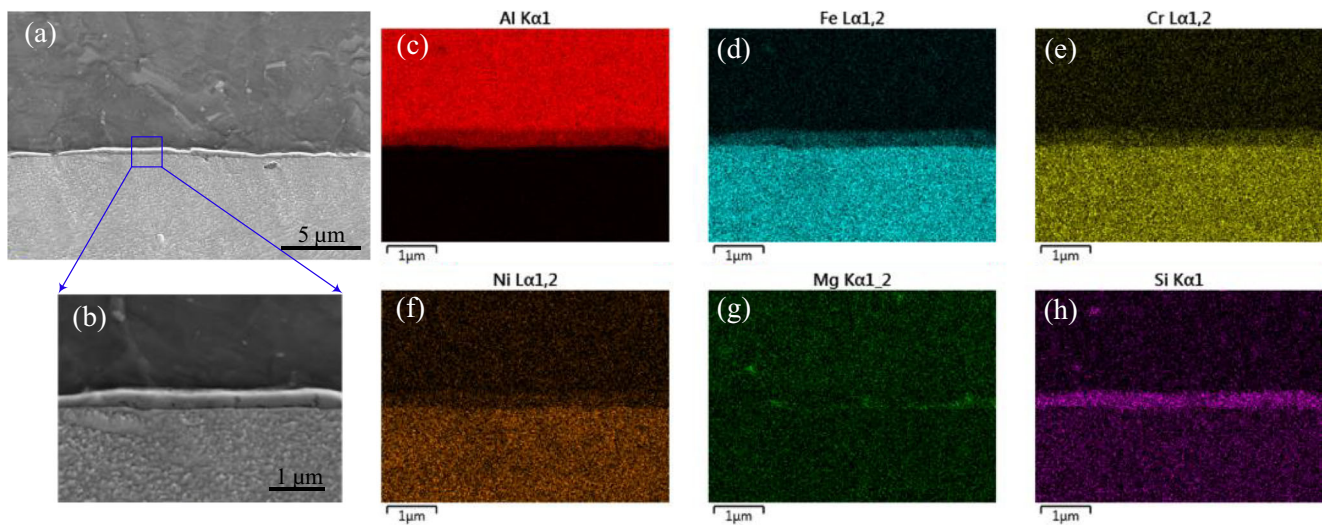


Fig. 4 a, b SEM images of the welding interface and c–h elemental mapping of Al/steel joint welded by CDFW

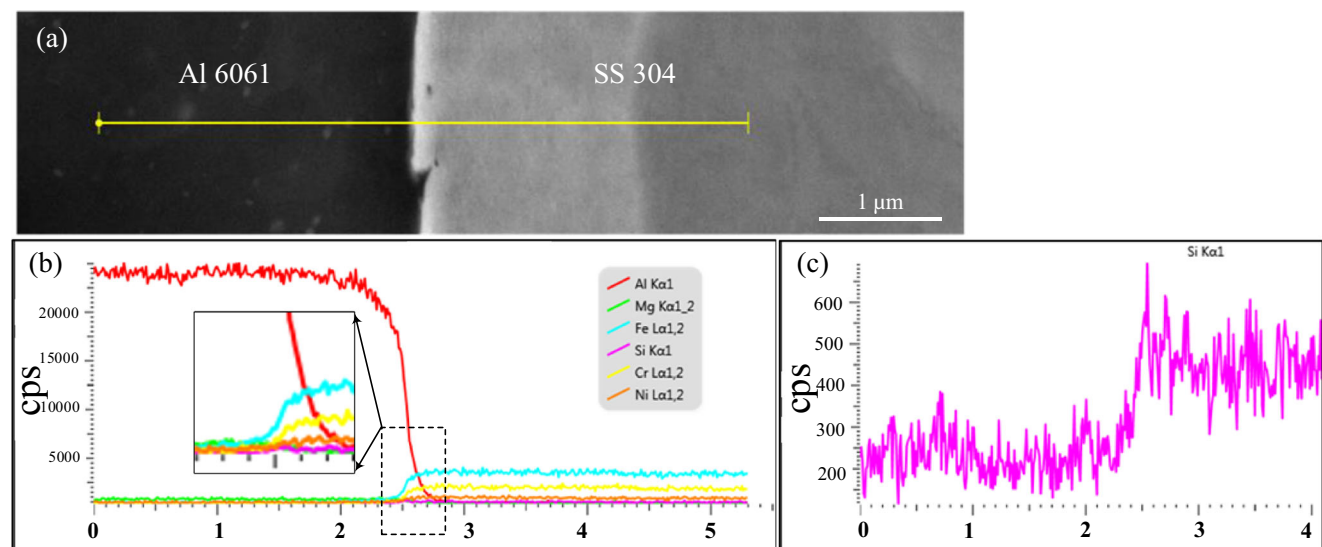


Fig. 5 a Welding interface and b, c EDS analysis of Al/steel joint welded by IFW

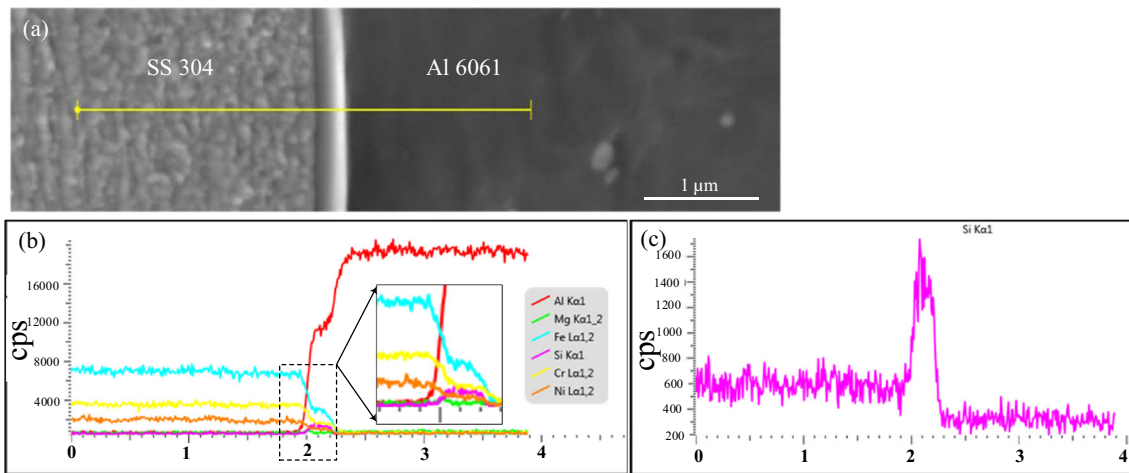


Fig. 6 a Welding interface and b, c EDS analysis of Al/steel joint welded by CDFW

interface. According to the Fig. 7 and chemical compositions (Table 3), the IMC should be Al₇Fe₂Si.

3.2 Microstructure of the welded joint

A clear weld interface was observed in the cross-section image, and the interface was relatively flat (Fig. 8). Typical friction welded joint consists of three distinct zones: (i) fully dynamic recrystallized zone (FDRZ), (ii) thermal

mechanically affected zone (TMAZ), and (iii) HAZ. The different temperature and strain histories of these zones affect the final microstructures.

3.2.1 The SS 304 side of Al/steel joint

Figure 8 shows the metallographic structure of the steel side in the Al/steel joint welded two methods. Few elongated grains are observed at the steel side. During friction welding, the

Fig. 7 a TEM images and b–d EDS analysis of Al/steel joint welded by IFW

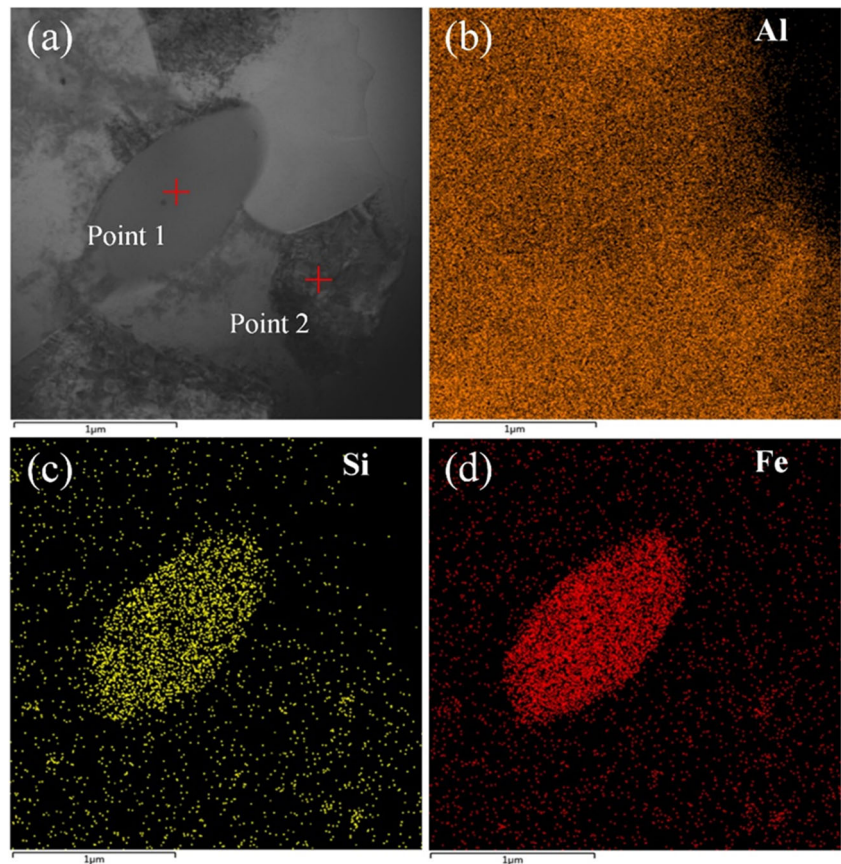


Table 3 The composition of position in Fig. 7 (wt.%)

Point	Al	Fe	Mg	Si	Cr	Mn	Ni
1	64.57	24.22	0.07	5.97	2.19	2.21	0.77
2	96.18	1.40	1.21	0.52	0.53	0.08	0.08

interface temperature rose rapidly due to thermal-mechanical coupling effect, which promoted aluminum alloy to experience recovery and dynamic recrystallization near the interface [27]. FDRZ was located close to the interface. It could be seen that the average width of FDRZ at steel side in the IFW joint was about 5 μm , while the average width of FDRZ in the CDFW joint was only 2 μm . FDRZ had changed the microstructure of fine equiaxed grains compared to the base metal, and the formation of fine equiaxed grains was clearly observed as a result of the frictional heat at the joint interface. The grain size of FDRZ was below 0.1 μm in both joints welded by two methods (Figs. 9 and 10).

3.2.2 The Al 6061 side of Al/steel joint

Figure 11 shows the metallographic structure of Al 6061. In TMAZ, grains were elongated and bended. Matrix grains deformed along TMAZ due to plastic flow. The direction of plastic flow was clear. A large number of streamlines were formed, resulting in the strengthened particle rearrangement.

Because the amount of second phase was high, the streamlines at the Al side were more dramatically than that at the steel side. Compared to the HAZ, the microstructure of the TMAZ underwent acute plastic deformation, inducing the appearance of deformed and elongated recrystallized grains. The grain sizes of both joints were found in the order of 1–3 μm , and the width of FDRZ in the Al side was almost zero (Figs. 12 and 13).

3.3 Hardness of the welded joint

Figure 14 shows the microhardness distribution of joints welded by two methods. Because physical and chemical properties of base metals were different, the hardness of SS 304 was about 3 times that of the Al 6061 base metal. The hardness reached to the maximum value in the FDRZ at the steel side. The high hardness located to the welding interface at the steel side in the CDFW joint. Microhardness of joints may be affected by a combination of some or all of the following factors: modification of microstructure, dissolution of strengthening phases, grain size, and IMC formation. Reasons should be related to the eutectics and recrystallized fine grains as an effect of heat input, rotational speed, the plastic deformation, and relative movement during upsetting/forging.

In addition, the narrow FDRZ in the IFW joint was hard to allow the microhardness measurement, which was also another reason for the relatively low maximum value in the IFW

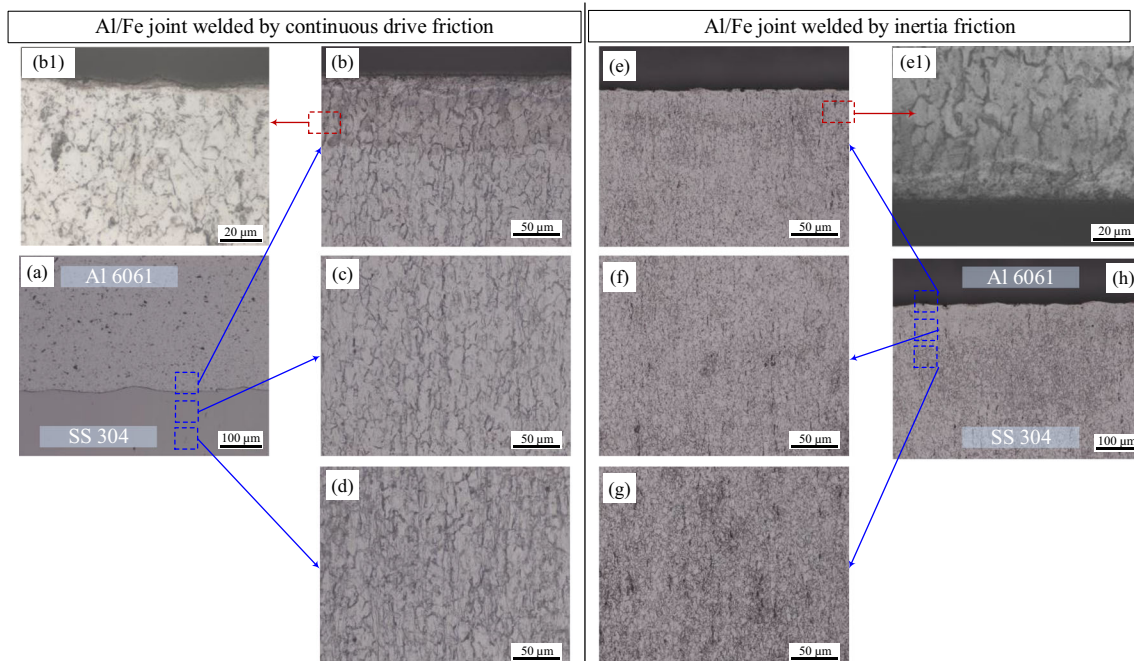
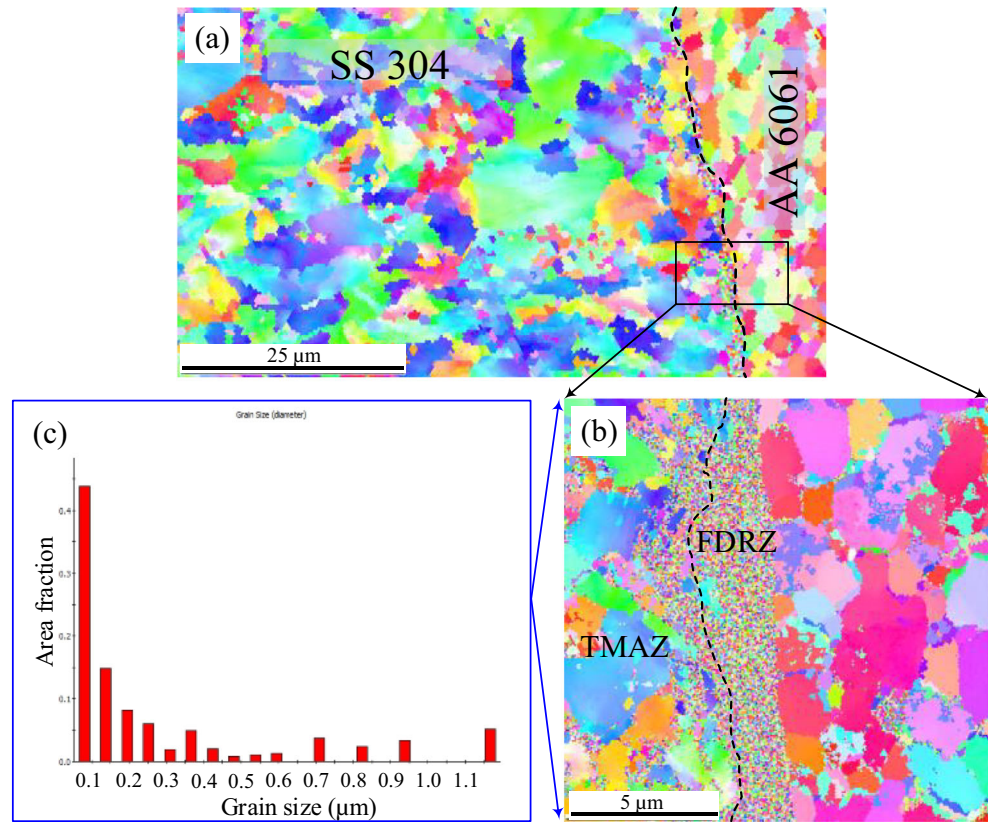


Fig. 8 Microstructure characteristic of the steel side in the Al/steel joint welded by two methods: **a–d** microstructure of the CDFWed joint and **e–h** microstructure of the IFWed joint

Fig. 9 a, b EBSD images and c grain size of TMAZ and HAZ at the steel side in the IFW joint



joint. In the Al base metal, the average hardness value was 101.5 HV, while the average hardness value of HAZ was 76 HV. Hardness depletion of the HAZ of heat treated 6061 (T6) was influenced by its thermal history.

3.4 Tensile strength of the welded joint

In the IFWed joint, the tensile strength gradually increased due to increased friction pressure, and reached to the

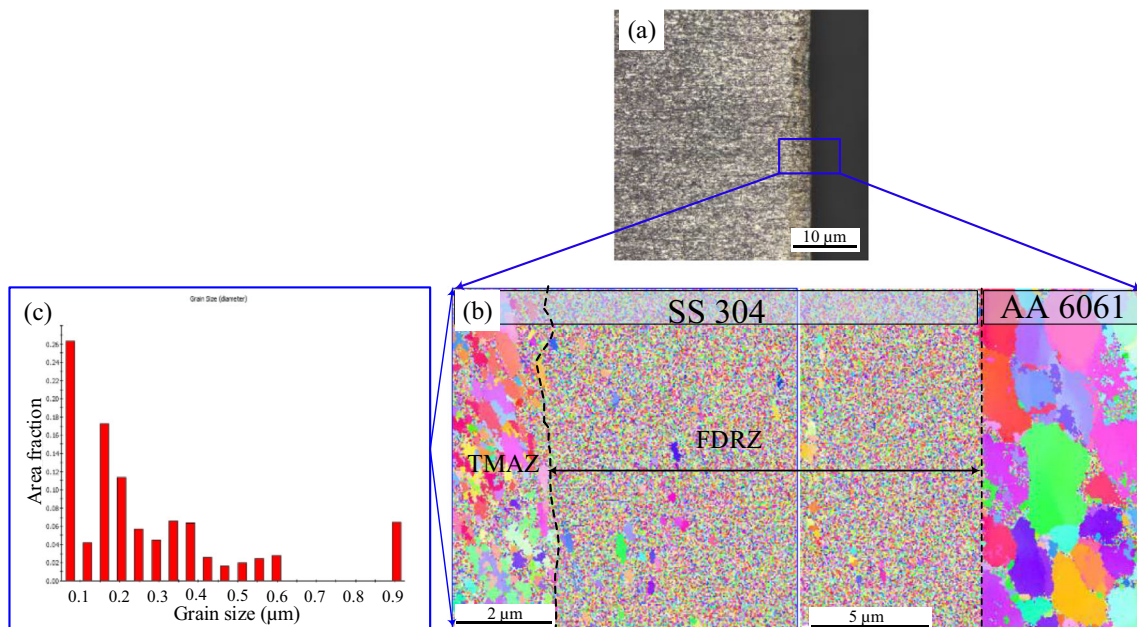


Fig. 10 a, b EBSD images and c grain size of TMAZ and HAZ at the steel side in the CDFW joint

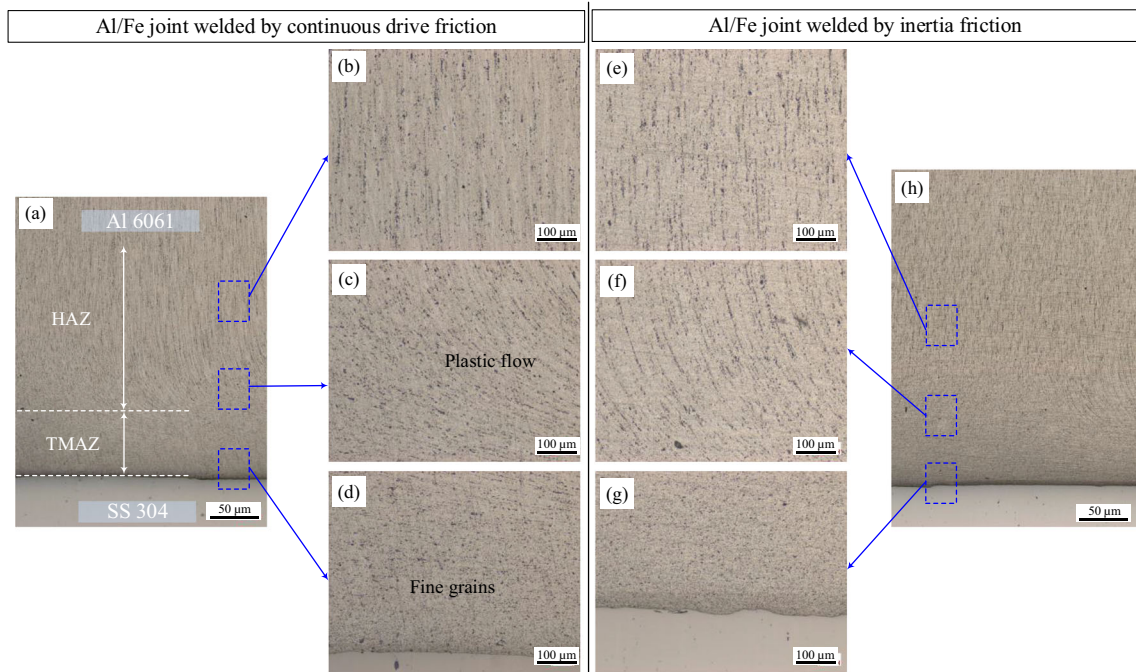


Fig. 11 Microstructure characteristic of the Al side in the Al/steel joint welded by two methods: **a–d** microstructure of the CDFWed joint and **e–h** microstructure of the IFWed joint

maximum tensile strength of 323 MPa, which was about 94% of Al 6061 base metal (Fig. 15a). If friction pressure was continued to increase, joint strength started to decrease. In the CDFWed joint, the tensile strength of joint first increased and then decreased with the increase of friction pressure (Fig. 15b). The joint average strength reached the maximum

value of 304 MPa. The maximum tensile strength of IFWed joint was higher than the maximum tensile strength of CDFWed joint, and the reason should be related to the thickness of IMC at the weld interface. The thick, continuous, and hard IMC layer would provide the potential initiation of crack, as shown in Fig. 15c. The thick layer of IMCs deteriorated the

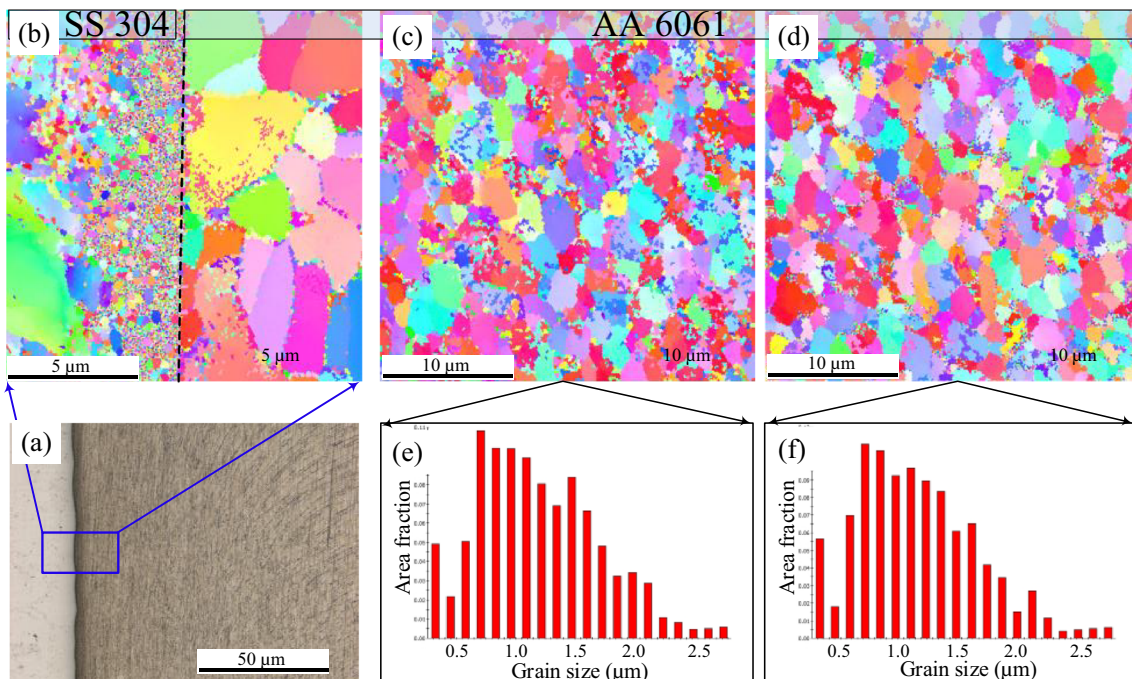


Fig. 12 **a** Measure position, **b–d** EBSD images, and **e–f** grain size of TMAZ and HAZ at the Al side in the IFWed joint

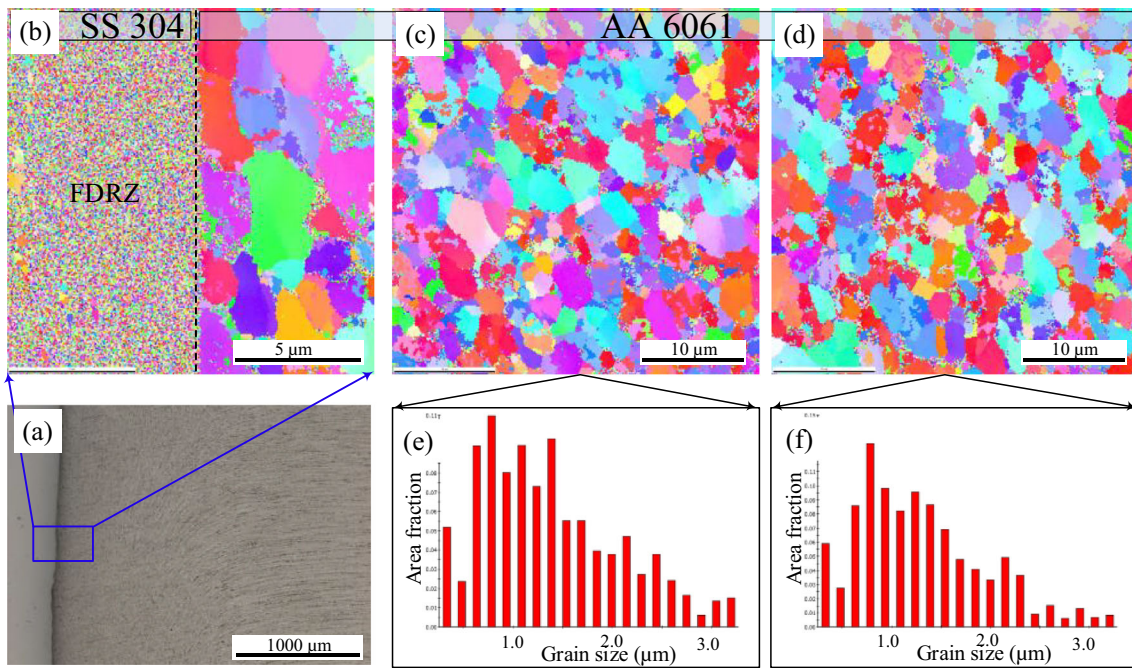


Fig. 13 a Measure position, b–d EBSD images, and e–f grain size of TMAZ and HAZ at the Al side in the CDFW joint

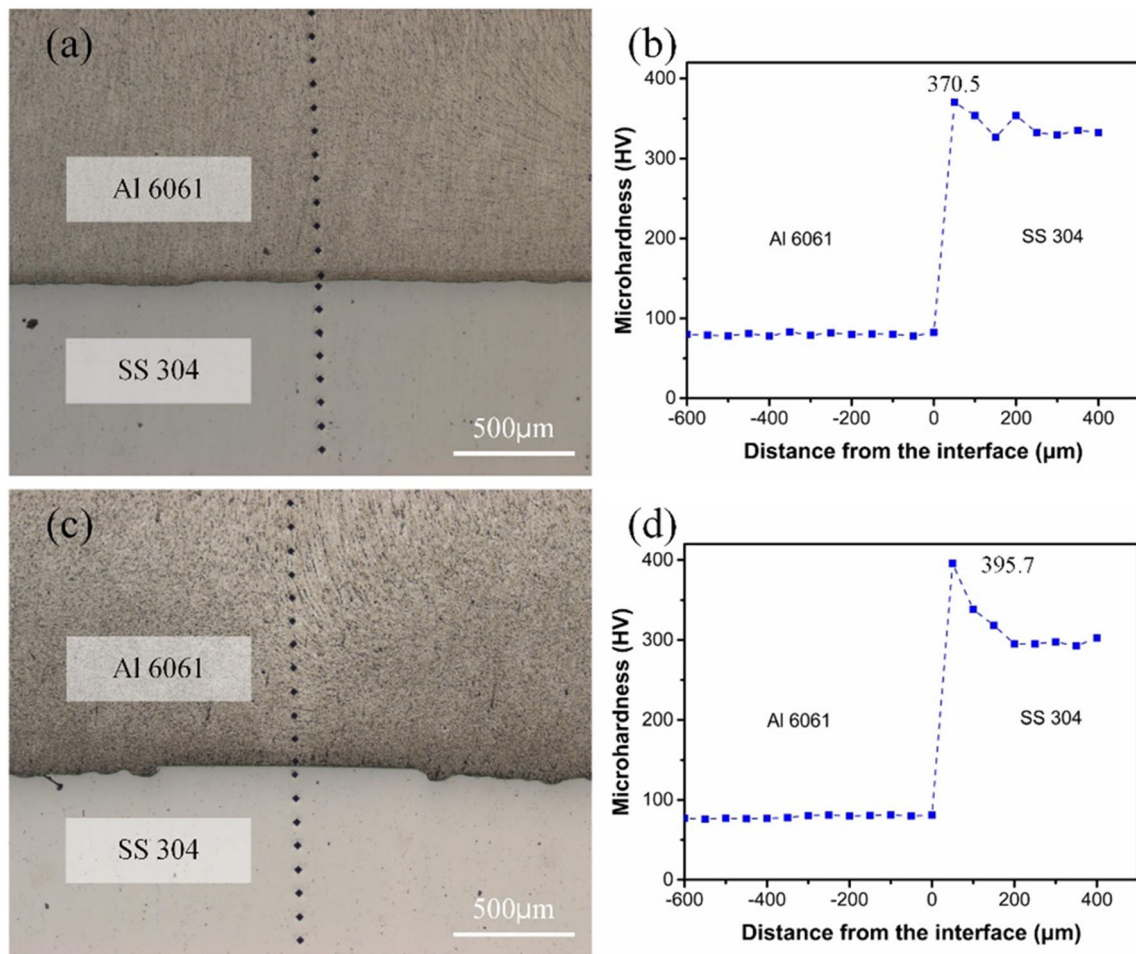


Fig. 14 Hardness of the welded joints. a, b Measured position and hardness distribution of CDFW joint. b–c Measured position and hardness distribution of IFW joint

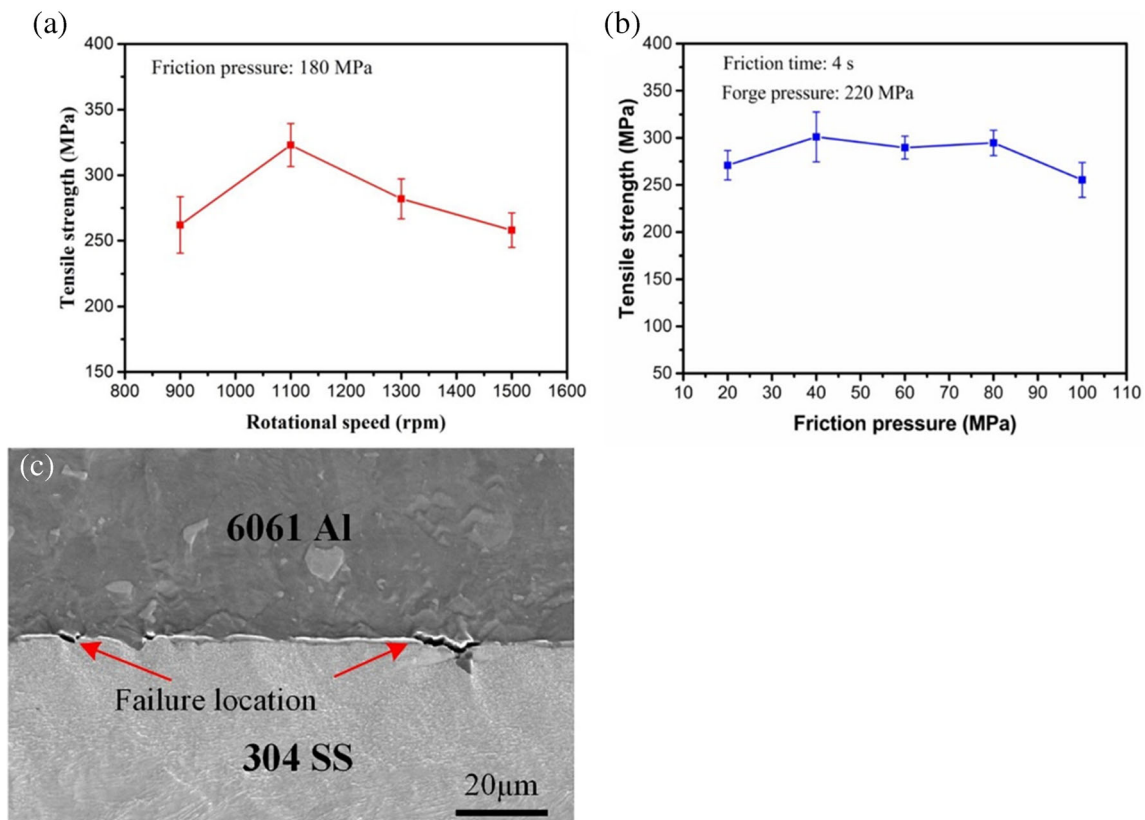


Fig. 15 **a** Influence of rotational speed on the tensile strength of the IFWeld joint. **b** Influence of friction pressure on the tensile strength of the CDFWeld joint. **c** The continuous IMC layer of the CDFWeld joint

tensile strength and ductility of the joint. The analysis of the Al-steel interface was considered as critical due to the formation of brittle IMCs at this location.

4 Conclusions

- (1) Al 6061 and SS 304 exhibited consistent flying edges at the interface in both joints. An average 600-nm thick reaction layer was found between stainless steel and aluminum alloy in the CDFWeld joint, which was wider and clearer than the IMC layer of the IFWeld joint. The high concentration level of Si was observed at the interface in both joints, and the presence of Si at a high concentration level could have promoted the formation of non-uniform IMC layer.
- (2) At the SS 304 side of Al/steel joint, few elongated grains are observed and FDRZ was located close to the interface. The average width of FDRZ at steel side in the IFW joint was about 5 μm, while the average width of FDRZ in the CDFW joint was only 2 μm. The grain size of FDRZ was below 0.1 μm in both joints welded by two methods. At the Al 6061 side of Al/steel joint, grains were elongated and bended, and the streamlines at the Al side were more dramatically than that at the steel side

in TMAZ. The grain size of both joints was almost the same and the width of FDRZ in the Al side was almost zero.

- (3) The high hardness located in the FDRZ at the steel side. The maximum tensile strength of IFWeld joint was higher than that of CDFWeld joint because of the different thickness of IMC at the weld interface. The thick, continuous, and hard IMC layer would provide the potential initiation of crack.

References

1. Shah LH, Ishak M (2014) Review of research progress on aluminum–steel dissimilar welding. *Mater Manuf Process* 29: 928–933
2. Aghajani Derazkola H, Khodabakhshi F (2019) Intermetallic compounds (IMCs) formation during dissimilar friction-stir welding of AA5005 aluminum alloy to St-52 steel: numerical modeling and experimental study. *Int J Adv Manuf Tech* 100:2401–2422
3. Wang P, Chen X, Pan Q, Madigan B, Long J (2016) Laser welding dissimilar materials of aluminum to steel: an overview. *Int J Adv Manuf Tech* 87:3081–3090
4. Huang Y, Wan L, Si X, Huang T, Meng X, Xie Y (2019) Achieving high-quality Al/steel joint with Ultrastrong Interface. *Metall Mater Trans A* 50:295–299

5. Sun G-Q, Xu G-S, Shang D-G, Chen S-J (2019) Welding parameter selection and short fatigue crack growth of dissimilar aluminum alloy friction stir welded joint. *Weld World* 64:1–9
6. Meshram SD, Mohandas T, Reddy GM (2007) Friction welding of dissimilar pure metals. *J Mater Process Tech* 184:330–337
7. Huang Y, Huang T, Wan L, Meng X, Zhou L (2019) Material flow and mechanical properties of aluminum-to-steel self-riveting friction stir lap joints. *J Mater Process Tech* 263:129–137
8. Yilmaz M, Çöl M, Acet M (2003) Interface properties of aluminum/steel friction-welded components. *Mater Charact* 49:421–429
9. Li W, Vairis A, Preuss M, Ma T (2016) Linear and rotary friction welding review. *Int Mater Rev* 61:71–100
10. Ding Y, You G, Wen H, Li P, Tong X, Zhou Y (2019) Microstructure and mechanical properties of inertia friction welded joints between alloy steel 42CrMo and cast Ni-based superalloy K418. *J Alloy Comp* 803:176–184
11. Preuss M, Withers PJ, Baxter GJ (2006) A comparison of inertia friction welds in three nickel base superalloys. *Mater Sci Eng A* 437:38–45
12. Zhang C, Shen W, Zhang L, Xia Y, Li R (2017) The microstructure and gamma prime distributions in inertia friction welded joint of P/M Superalloy FGH96. *J Mater Eng Perform* 26:1581–1588
13. Wang FF, Li WY, Li JL, Vairis A (2014) Process parameter analysis of inertia friction welding nickel-based superalloy. *Int J Adv Manuf Tech* 71:1909–1918
14. Turner RP, Perumal B, Lu Y, Ward RM, Basoalto HC, Brooks JW (2019) Modeling of the heat-affected and thermomechanically affected zones in a Ti-6Al-4V inertia friction weld. *Metall Mater Trans B Process Metall Mater Process Sci* 50:1000–1011
15. Guo W, You G, Yuan G, Zhang X (2017) Microstructure and mechanical properties of dissimilar inertia friction welding of 7A04 aluminum alloy to AZ31 magnesium alloy. *J Alloy Comp* 695:3267–3277
16. Luo J, Liu S, Chen W, Xu X (2016) Friction interface migration of copper alloy and carbon steel dissimilar metal joints in inertia radial friction welding. *Mater Manuf Process* 31:275–282
17. Ahmad Fauzi MN, Uday MB, Zuhailawati H, Ismail AB (2010) Microstructure and mechanical properties of alumina-6061 aluminum alloy joined by friction welding. *Mater Des* 31:670–676
18. Mehta KP (2019) A review on friction-based joining of dissimilar aluminum–steel joints. 34:78–96
19. Maalekian M (2007) Friction welding – critical assessment of literature. *Sci Technol Weld Joi* 12:738–759
20. Luo J, Ye YH, Xu JJ, Luo JY, Chen SM, Wang XC, Liu KW (2009) A new mixed-integrated approach to control welded flashes forming process of damping-tube–gland in continuous drive friction welding. *Mater Des* 30:353–358
21. Wan L, Huang Y (2018) Friction welding of AA6061 to AISI 316L steel: characteristic analysis and novel design equipment. *Int J Adv Manuf Tech* 95:4117–4128
22. Li P, Li J, Li X, Xiong J, Zhang F, Liang L (2015) A study of the mechanisms involved in initial friction process of continuous drive friction welding. *J Adhes Sci Technol* 29:1246–1257
23. Kimura M, Ishii H, Kusaka M, Kaizu K, Fuji A (2009) Joining phenomena and joint strength of friction welded joint between aluminium–magnesium alloy (AA5052) and low carbon steel. *Sci Technol Weld Joi* 14:655–661
24. James JA, Sudhish R (2016) Study on effect of interlayer in friction welding for dissimilar steels: SS 304 and AISI 1040. *Proc Technol* 25:1191–1198
25. Kimura M, Kusaka M, Kaizu K, Nakata K, Nagatsuka K (2016) Friction welding technique and joint properties of thin-walled pipe friction-welded joint between type 6063 aluminum alloy and AISI 304 austenitic stainless steel. *Int J Adv Manuf Tech* 82:489–499
26. Herbst S, Aengeneyndt H, Maier HJ, Nürnberger F (2017) Microstructure and mechanical properties of friction welded steel-aluminum hybrid components after T6 heat treatment. *Mater Sci Eng A* 696:33–41
27. Dong H, Li Y, Li P, Hao X, Xia Y, Yang G (2019) Inhomogeneous microstructure and mechanical properties of rotary friction welded joints between 5052 aluminum alloy and 304 stainless steel. *J Mater Process Tech* 272:17–27
28. Fukumoto S, Tsubakino H, Okita K, Aritoshi M, Tomita T (2000) Amorphization by friction welding between 5052 aluminum alloy and 304 stainless steel. *Scripta Mater* 42:1–5
29. Fukumoto S, Tsubakino H, Okita K, Aritoshi M, Tomita T (1999) Friction welding process of 5052 aluminium alloy to 304 stainless steel. *Mater Sci Tech* 15:1080–1086

Publisher's note Springer Nature remains neutral with regard to jurisdictional claims in published maps and institutional affiliations.